Polymer 150 (2018) 26–34

Contents lists available at ScienceDirect

Polymer

journal homepage: www.elsevier.com/locate/polymer

Surface-initiated RAFT polymerization from vapor-based polymer coatings

Gowthamy Venkidasubramonian [a, 1], Domenic Kratzer [a, 1], Vanessa Trouillet [b], Nicolas Zydziak [c], Matthias Franzreb [a], Leonie Barner [a, c, d, *], Joerg Lahann [a, c, e, **]

[a] Institute of Functional Interfaces (IFG), Karlsruhe Institute of Technology (KIT), Hermann-von-Helmholtz-Platz 1, 76344, Eggenstein-Leopoldshafen, Germany
[b] Institute for Applied Materials (IAM) and Karlsruhe Nano Micro Facility (KNMF), Karlsruhe Institute of Technology (KIT), 76344, Eggenstein-Leopoldshafen, Germany
[c] Soft Matter Synthesis Laboratory, Institute for Biological Interfaces 3 (IBG 3), Hermann-von-Helmholtz-Platz 1, 76344, Eggenstein-Leopoldshafen, Germany
[d] School of Chemistry, Physics and Mechanical Engineering, Queensland University of Technology (QUT), 2 George Street, QLD, 4000, Brisbane, Australia
[e] Biointerfaces Institute and Departments of Chemical Engineering, Materials Science and Engineering, Macromolecular Science and Engineering and Biomedical Engineering, University of Michigan, Ann Arbor, MI, 48109, USA

ARTICLE INFO

Article history:
Received 26 March 2018
Received in revised form
22 June 2018
Accepted 25 June 2018
Available online 27 June 2018

Keywords:
Chemical vapor deposition polymerization
"Clickable" chain transfer agent (CTA)
Surface-initiated reversible addition-fragmentation chain transfer (SI-RAFT) polymerization
Graft polymers
Reversible deactivation radical polymerization (RDRP)

ABSTRACT

Surface-initiated reversible addition-fragmentation chain transfer (SI-RAFT) polymerization was used to synthesize poly(methyl methacrylate) (PMMA) and poly[2-(methacryloyloxy)ethyl]dimethyl-(3-sulfopropyl)ammoniumhydroxide (PMEDSAH) brushes grafted from reactive poly[*p*-xylylene] surfaces. The synthetic approach involved functionalization of substrates via chemical vapor deposition polymerization of an electron-deficient alkynyl-functionalized [2.2]paracyclophane derivative. An azide-functionalized RAFT agent was anchored to the resulting poly[(*p*-xylylene-4-methyl propiolate)-co-*p*-xylylene] films *via* copper-free click-chemistry. Subsequent SI-RAFT polymerization yielded PMMA and PMEDSAH films with narrow dispersity which was further tuned by varying the concentration of a sacrificial RAFT agent in solution. Polymer dispersity was determined by size exclusion chromatography to be in the range of 1.2–1.4 for both polymers. This work provides a novel surface modification strategy to decorate a wide range of different substrates with polymer brushes, thereby eliminating the need for cumbersome modification protocols, which so far had to be established for each substrate material independently.

1. Introduction

Well-defined interfaces featuring synthetic polymer coatings are becoming increasingly important for numerous pharmaceutical and biotechnological applications including medical implants, drug delivery systems and tissue engineering scaffolds [1–3]. Synthetic coatings can be prepared by the adsorption of Langmuir-Blodgett layers, layer-by-layer assembly or through covalent bonding of polymer chains [4–6]. The "grafting-from" technique, *i.e.*, the synthesis of polymers directly from surface-immobilized initiators, has become a powerful method to modify organic and inorganic surfaces, by controlling length, architecture and composition [7,8]. Controlled polymerization techniques are particularly attractive for the preparation of surface-grafted polymer brushes, as they allow for accurate control over thickness and architecture [9]. Recent developments in the field of surface-initiated reversible deactivation radical polymerization (SI-RDRP), like atom transfer radical polymerization (ATRP), nitroxide-mediated radical polymerization (NMP), photoiniferter-mediated polymerization (PIMP) or reversible addition-fragmentation chain transfer (RAFT) polymerization have allowed the preparation of stable polymer films with tailored

* Corresponding author. School of Chemistry, Physics and Mechanical Engineering, Queensland University of Technology (QUT), 2 George Street, QLD, 4000, Brisbane, Australia.
** Corresponding author. Institute of Functional Interfaces (IFG), Karlsruhe Institute of Technology (KIT), Hermann-von-Helmholtz-Platz 1, 76344, Eggenstein-Leopoldshafen, Germany.
E-mail addresses: leonie.barner@qut.edu.au (L. Barner), lahann@umich.edu (J. Lahann).
[1] These authors contributed equally to this work.

https://doi.org/10.1016/j.polymer.2018.06.073
0032-3861/

surface properties [5,10].

Among the different SI-RDRP techniques available, ATRP is likely the most prominent strategy used for the synthesis of polymer brushes [5,11,12]. An alternative strategy involves the RAFT polymerization process [13–17] gaining popularity over the past decade due to its relative ease of use and mild reaction conditions [18]. Surface-initiated RAFT polymerization with a sacrificial chain transfer agent (CTA) has been an efficient method to synthesize polymer films with controlled thickness and composition [19]. The presence of a free CTA in solution effectively controls the concentrations of dormant and propagating chains on the surface by the exchange reactions between surface and free radicals.

Several methods have been reported for the immobilization of CTA onto surfaces. For instance, RAFT-silane agents can be covalently bound to silicon surfaces [20]. Zamfir et al. [21], carried out RAFT polymerization of 2-hydroxyl methacrylate (HEMA) from surface-functionalized RAFT-silane agents. They observed a marked effect of the sacrificial CTA concentration on the thickness of the polymer films. Re-initiation of the PHEMA polymerization demonstrated its living nature. However, the hydrolytic stability of siloxanes on inorganic surfaces remains a critical issue due to the polar nature of the Si-O-metal bond [22]. Self-assembled monolayers (SAMs) have also become a popular technique to introduce CTA on surfaces, but are limited to specialized substrates such as gold or silicon [23]. Another approach is the immobilization of the CTA by an indirect method that involves conversion of a surface-bound ATRP initiator into a CTA [24]. The CTA can also be anchored by UV-triggered photoreaction [25] or electrodeposition [26]. Recently, Kuliasha et al. [27] tailored the surface properties of poly(dimethylsiloxane) (PDMS) utilizing photografting of benzophenone, and then used the RAFT strategy to polymerize acrylate/methacrylate monomers. However, this strategy for RAFT polymerization is limited to polymer substrates.

Chemical vapor deposition (CVD) polymerization of substituted paracyclophanes is a proven technology that can produce thin, homogeneous and high density reactive polymeric films on a broad variety of materials [28–31]. Some members of the poly-*p*-xylylene family (trade name: parylene) have gained commercial acceptance due to their high solvent resistance, low dielectric constants, and good barrier properties [32,33]. They are extensively used as a barrier medium for implantable chemical sensors [34], stainless steel implants [35], pacemakers [36], stents and catheters [37]. The CVD process yields conformal coatings with pinhole-free coverage and can also be applied to complex 3-dimensional geometries [38]. A range of functionalized coatings such as nucleophiles (amines and alcohols), electrophiles (aldehydes), or maleimides have been reported [39–43].

Alkyne functionalized [2.2]paracyclophanes were successfully polymerized via the CVD route on a wide range of different substrates and can even support micro- and nanopatterning by orthogonal reaction with azides [44]. Activated alkynes react with azide groups in a so-called click reaction that proceeds even in the absence of a transition metal catalyst [45]. In the current work, we utilize the CVD polymerization of alkyne functionalized parylenes to prepare reactive surfaces, which are used to immobilize an azide-functionalized RAFT agent. Polymer brushes from methyl methacrylate (MMA) and 2-methacryloyloxyethyldimethyl-3-sulfopropyl ammonium hydroxide (MEDSAH) are then grafted from these surfaces via RAFT polymerization. In particular, the zwitterionic PMEDSAH brushes have excellent anti-fouling and anti-bacterial properties [46]. Previous studies showed that PMEDSAH polymer coatings further support long term growth of human embryonic stem cells [47]. CVD polymerization of alkyne-functionalized reactive coatings have been successfully deposited on a range of inorganic and organic surfaces in our previous work [44]. We now extend our efforts to immobilize CTAs on these reactive polymer coatings and demonstrate their use in RAFT polymerization.

2. Materials and methods

2.1. Materials

4-Cyano-4-(phenylcarbonothioylthio)pentanoic acid (CPA, 97%, Sigma Aldrich), *N,N′*-diisopropylcarbodiimide (DIC, 99%, Sigma Aldrich), *N,N′*-dicyclohexylcarbodiimide (DCC, 99%, VWR International), propiolic acid (95%, VWR International), sodium azide (99.5%, Sigma Aldrich), 3-bromopropan-1-ol (97%, Sigma Aldrich), magnesium sulfate anhydrous ($MgSO_4$, 97%, Sigma Aldrich), 4-dimethylaminopyridine (98%, Merck), 2,2,2-trifluoroethanol (TFE, 99%, Merck), ethanol (ACS reagent, 99.5% absolute, Alfa Aesar), dichloromethane (DCM, 99.8%, extra dry over molecular sieves, stabilized, Arcos Organics), ethyl acetate (ACS reagent, 99.5%, Alfa Aesar), acetone (ACS reagent, Alfa Aesar), *N,N*-dimethylformamide (DMF, Alfa Aesar), chloroform (Alfa Aesar), acetonitrile (Alfa Aesar), tetrahydrofuran (THF, 99%, stabilized with 250–350 ppm BHT, Alfa Aesar), methanol (Alfa Aesar), hexane (Alfa Aesar), sodium bicarbonate (ACS grade, Amresco), sodium bromide (Fluka), sodium chloride (NaCl, VWR International) and [2.2]paracyclophane (PCP, Curtiss Wright Surface Technologies, Galway, Ireland) were used as received. Azobisisobutyronitrile (AIBN, 98%, Sigma Aldrich) and 4,4′-azobis(4-cyanovaleric acid) (V501, 75%, Sigma Aldrich) were purified by recrystallization from methanol and stored at −20 °C. Methyl methacrylate (MMA, 99%, Merck) was passed through a basic alumina column to remove the inhibitor. Silicon wafers with a native oxide layer (Siegert Wafer GmbH, Aachen, Germany) were cut into $10 \times 10\ mm^2$ pieces using a diamond-tipped cutter. Gold wafers were prepared on silicon wafers by physical vapor deposition, with 5 nm titanium seed layer followed by 100 nm of gold.

2.2. Characterization

2.2.1. Infrared reflection absorption spectroscopy (IRRAS)

IRRAS was performed on a Bruker VERTEX 80 V spectrometer equipped with a liquid-nitrogen cooled MIR MCT detector at a grazing angle of 80°. The IRRAS spectra were recorded using 5 cm^{-1} resolution. The resulting spectra were corrected for any residual baseline shifts.

2.2.2. Water contact angle (WCA)

Contact angles were determined by the static sessile water drop contact angle method using a Krüss DSA 100. The droplet volume was 10 μL. The statistical analysis was performed with Origin. Significance was calculated using a Student's *t*-test; only P values ≤ 0.05 were considered statistically significant.

2.2.3. Ellipsometry

Ellipsometric measurements were performed on an M44 multi-wavelength rotating analyzer ellipsometer (J.A. Woollam, USA) in the wavelength range of $\lambda = 280–800$ nm at an incident angle of 65°. The organic layers were modeled with the CompleteEASE software (J.A. Woollam) as a Cauchy layer. For the calculation of the layer thickness, refractive index values of $n = 1.65$ (for the CVD layer), $n = 1.5$ (for PMMA) and $n = 1.58$ (for PMEDSAH) were used. The data points were the average of two independent trials.

2.2.4. X-ray photoelectron spectroscopy (XPS)

XPS data were recorded with a K-Alpha XPS spectrometer (ThermoFisher Scientific, East Grinstead, UK). Data acquisition and processing were performed using the Thermo Avantage software as

described elsewhere [48]. All thin films were analyzed using a microfocused, monochromated Al Kα X-ray source (400 μm spot size). A K-Alpha charge compensation system was employed during analysis using electrons of 8 eV energy and low-energy argon ions to prevent any localized charge build-up. The spectra were fitted with one or more Voigt profiles (binding energy uncertainty: ±0.2 eV) and Scofield sensitivity factors were applied for quantification [49]. All spectra were referenced to the C 1s signal (C–C, C–H) at 285.0 eV binding energy controlled by means of the well-known photoelectron signals of metallic Cu, Ag and Au respectively. The random error associated with quantitative elemental analysis was between 5 and 10%.

2.2.5. Size exclusion chromatography (SEC)

SEC with THF as eluent was performed on a Tosoh Bioscience instrument (model EcoSEC), using a differential refractive index detector at 30 °C with a flow rate of 1 mL min^{-1}. The three SDV columns (dimensions: 100 Å, 5 μm, 8 × 300 mm; 1000 Å, 5 μm, 8 × 300 mm; 100000 Å, 5 μm, 8 × 300 mm) from PSS were calibrated against linear poly(methyl methacrylate) (800-1.82 × 10^6 g mol^{-1}) and linear poly(styrene) (266-2.52 × 10^6 g mol^{-1}), respectively. SEC with 80% 0.5 M NaBr/20% acetonitrile as eluent was performed on a SECcurity GPC System equipped with a Novema 10 μm bead-size guard column and a refractive index detector. Linear polyethylene glycol (PEG) standards were used to generate the calibration curve (232–1015000 g mol^{-1}).

2.2.6. Atomic force microscopy (AFM)

The surface morphology of the substrates was evaluated by AFM using an Asylum Research (USA) instrument in tapping mode under ambient conditions. All values are recorded for a 2 × 2 μm^2 area. Statistical analysis was performed as described above (WCA section).

2.3. Methods

All experimental details and results of the synthesis of the CVD precursor PCP-alkyne, RAFT agent Azido-CTA and MEDSAH are presented in the supplementary material section.

CVD polymerization of PCP-alkyne. CVD polymerization used a custom-built CVD system that ensured the slow sublimation of 80 mg of precursor PCP-alkyne at 100–120 °C under reduced pressure of 0.1 mbar. The vaporized dimers were subsequently transferred into the pyrolysis zone, which was heated to 510 °C, with 20 sccm argon as carrier gas, where the precursor was transformed into reactive species (*p*-quinodimethanes). Finally, deposition of poly[(*p*-xylylene-4-methyl-propiolate)-co-(*p*-xylylene)] (PPX-alkyne) onto the substrate occurred on a temperature-controlled rotating sample holder (15 °C) in the deposition chamber with a wall temperature of 90 °C. The CVD deposition rate was kept at 0.1 Å/s and was monitored *in situ* by a quartz crystal microbalance (QCM).

Copper-free click-chemistry on PPX-alkyne surfaces: Immobilization of the azido-CTA on the PPX-alkyne reactive polymer coating was achieved as follows: 0.01 M of the azido-CTA dissolved in ethanol was introduced onto PPX-alkyne surface. The substrate was placed under argon at 50 °C for 48 h. After the reaction, the surface-modified reactive polymer coating was thoroughly washed with copious amounts of ethyl acetate followed by ethanol to remove the residual azido-CTA. Finally, the CTA-modified reactive polymer coating (S-CTA) was dried and stored under argon. The surfaces were then characterized by ellipsometry and XPS.

Surface-initiated RAFT Polymerization of MMA. In a typical procedure, a two-neck round bottom flask was charged with MMA (4 mol L^{-1}), free RAFT agent CPA (3 mmol L^{-1} or 8.7 mmol L^{-1}), AIBN (3 mmol L^{-1}) and DMF (1.3 mL per 1 mL monomer). The solution was degassed by three consecutive freeze-pump-thaw-cycles. A total volume of 2 mL of this mixture was transferred into each of 6 dried and purged vials containing functionalized substrates, S-CTA, under argon atmosphere. All vials were placed in a preheated oil bath at 70 °C. At designated time intervals, each vial was removed, and the contents were analyzed. Conversion was analyzed by ^{1}H NMR spectroscopy using DMF as a reference. For SEC characterization, the reaction mixture was precipitated into ethyl ether twice for purification and filtered through a 0.2 μm syringe filter. Following polymerization, the modified substrates were washed three times with DMF, chloroform, acetone and dried under argon. Typical polymerization times for PMMA brushes were 1–6 h.

Surface-initiated RAFT Polymerization of MEDSAH. A solution of MEDSAH (0.1 g L^{-1}), free RAFT agent CPA (0.5 mmol L^{-1}), V-501 (0.05 mmol L^{-1}) and a 1:1 TFE/water (v/v) mixture was prepared in a two-neck round bottom flask. The mixture was degassed by three consecutive freeze-pump-thaw cycles, backfilled with argon and then transferred into each of 4 degassed Schlenk tubes containing the functionalized substrates S-CTA (3 mL/substrate). The reactions were carried out in a preheated oil bath at 80 °C. At designated time intervals, one vial was removed to determine percent monomer conversion and molecular weight of the polymer in solution. Following polymerization, the modified substrates were washed with TFE, water and dried in a stream of argon. The polymer in solution was dialyzed against water and freeze dried for purification. Typical polymerization times for PMEDSAH brushes were 2–8 h.

3. Results and discussion

Scheme 1 presents the research strategy employed for the fabrication of the PMMA and PMEDSAH polymer brushes on reactive polymer coatings. First, the reactive surface coatings functionalized with alkyne groups, poly[(*p*-xylylene-4-methyl propiolate)-co-*p*-xylylene] (PPX-alkyne) were polymerized by CVD polymerization. The azido-CTA was then immobilized on these surfaces by copper-free click reaction. SI-RAFT polymerization of MMA (used as a model monomer) and PMEDSAH from S-CTA surfaces was performed in the presence of a free RAFT agent CPA.

Alkyne-functionalized surfaces (PPX-alkyne). PPX-alkyne films were prepared using CVD polymerization of PCP-alkyne (Scheme 1) [50]. During CVD polymerization, ring-constrained PCP-alkyne was sublimed at 100–120 °C and 0.1 mbar, then thermally converted into quinodimethanes at 510 °C and transferred to the deposition chamber. Next, the quinodimethanes spontaneously polymerized upon adsorption onto the temperature-controlled substrate, resulting in homogenous coating of the sample. The resulting film thickness of the alkyne coatings used for the experiments was ~25 nm as measured by ellipsometry. This thickness was chosen to ensure pinhole-free surface coverage and compatibility with the XPS analysis (information depth 10–20 nm) [51]. Fig. 1a displays IRRAS spectra of PPX-alkyne coatings. Characteristic vibrational modes at 1719 cm^{-1} associated with the carbonyl group and at the C–O stretching band at 1222 cm^{-1} were detected. The signal of the terminal alkyne C≡C stretching vibrations at 2118 cm^{-1} and –C≡C–H stretching vibrations at 3284 cm^{-1} was also detected [50].

Additionally, XPS was used to quantitatively analyze the carbon and oxygen content of the coatings. The C 1s spectrum demonstrated the presence of aliphatic and aromatic carbons around 285.0 eV (a weak π-π* transition at ~291 eV) and C–O and O–C=O components at 286.7 eV and 289.2 eV, respectively [50]. The analysis indicates a composition of 88 ± 5 atomic percent (at%) carbon and 12 ± 2 at% oxygen which are in close agreement with

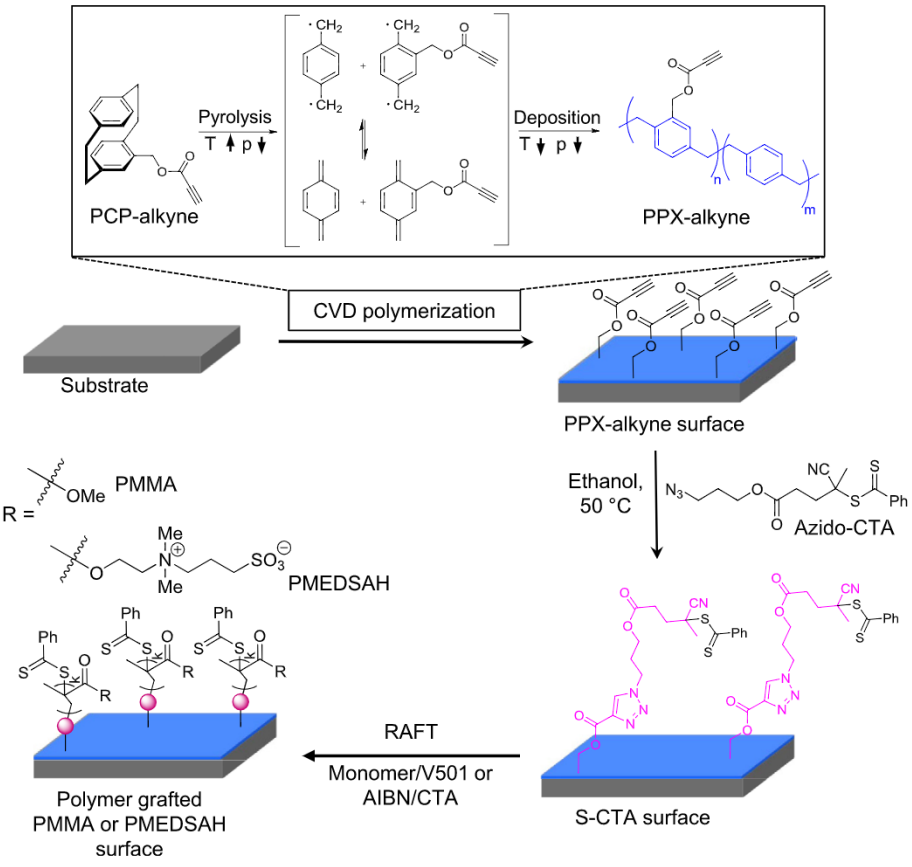

Scheme 1. Schematic illustration of the processes of CVD polymerization and the immobilization of the azide-functionalized CTA (azido-CTA) by copper-free click reaction on the alkyne-functionalized reactive polymer coatings (PPX-alkyne surface). During the CVD polymerization process, sublimation occurred for PCP-alkyne at approximately 100–120 °C. The sublimed paracyclophane was transferred from the source to the pyrolysis zone and exposed to elevated temperatures of 510 °C to thermally convert them into quinodimethanes. Finally, the quinodimethanes spontaneously polymerized upon condensation on a cooled (15 °C) substrate to generate PPX-alkyne surfaces. The surface-initiated RAFT polymerization of monomers from the RAFT agent-decorated surface (S-CTA) followed.

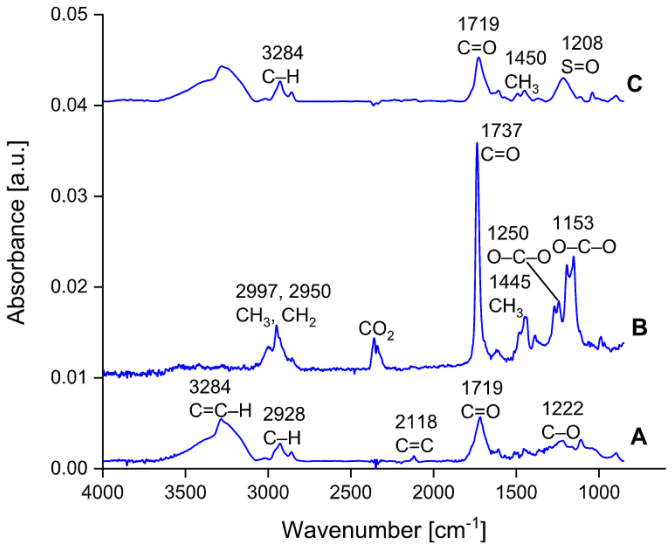

Fig. 1. Infrared reflection absorption spectra of the (A) reactive polymer coating (PPX-alkyne surface), (B) PMMA surface and (C) PMEDSAH surface.

theoretical values (Fig. S6, ESI†). Results of both the IRRAS and XPS data confirm the successful synthesis of PPX-alkyne surface. In the following, the PPX-alkyne surfaces were functionalized with azido-CTA to obtain the S-CTA surface.

Immobilization of azido-CTA onto PPX-alkyne surfaces: The azido-CTA was "clicked" to the alkyne groups via a copper-free Huisgen 1,3-dipolar cycloaddition. To confirm the functionalization, XPS measurements were performed. Fig. 2 compares the high-resolution N 1s and S 2p XPS spectra (from bottom to top) of PPX-alkyne coating before and after the reaction of the alkyne groups with azido-CTA. Before the reaction, nitrogen was not detected. After the reaction with azido-CTA, the N 1s peak was fitted with two components attributed to the triazole species. The signals at 401.8 and 400.2 eV correspond to the single bond and double bond nitrogen of the N=N–*N* respectively [52,53]. The elemental ratio for the nitrogen atoms is 1.3:2, compared to the calculated value of 1:2. Furthermore, the absence of an azide signal at ~405 eV indicates the absence of nonspecific adsorption of azides during the reaction. Additionally, no S 2p signal was detected on PPX-alkyne surface before the reaction in the high-resolution S 2p spectrum. After the click reaction, the S 2p spectrum can be deconvoluted into two main signals (Fig. 2b). The S 2p core-level spectrum consists of a spin-orbit doublet with S $2p_{3/2}$ and S $2p_{1/2}$. The S $2p_{3/2}$ at 162.8 eV corresponds to a covalently bonded C=*S* sulfur group and the peak at 164.2 eV corresponds to the covalently bonded C–S sulfur group [54]. Overall, the high-resolution XPS spectrum affirmed successful immobilization of the azido-CTA.

SI-RAFT polymerization from the S-CTA immobilized on reactive polymer coatings. Once the polymerization is initiated, two important events are considered: (1) the polymerization of the

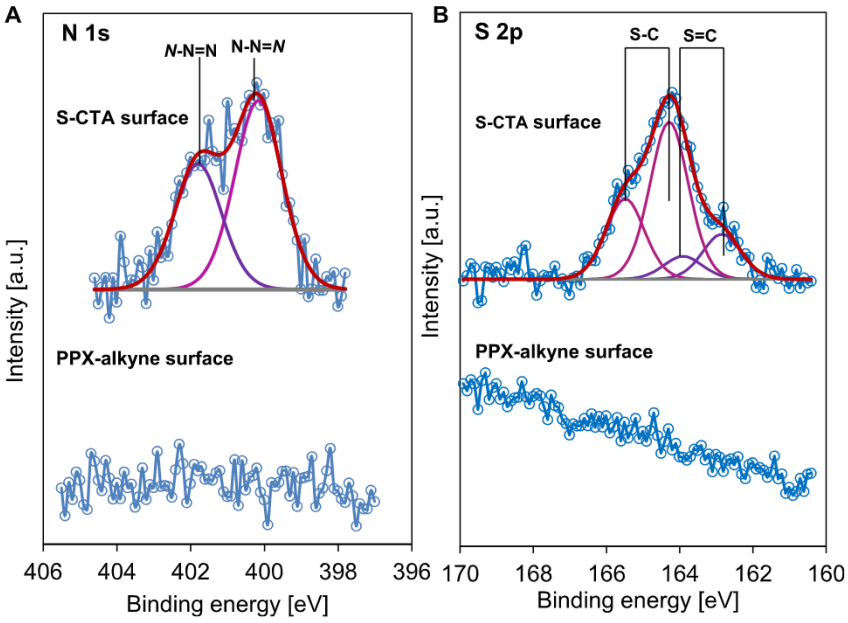

Fig. 2. (A) N 1s and (B) S 2p high-resolution XPS spectra of the PPX-alkyne reactive polymer coating and the S-CTA.

monomer from the substrate to obtain polymer brushes and (2) the polymerization of monomer simultaneously in solution. It is important to note that CPA is present in solution in addition to the immobilized RAFT agent on the substrate [21]. The addition of a "sacrificial" RAFT agent to the solution phase has been shown to improve the molecular weight control of the polymer brushes on surfaces [55,56]. The RAFT agent reacts reversibly with propagating polymer radicals to form dormant polymeric chains. The continuous reversible deactivation process mediated by a constant exchange between dormant and propagating polymer chains and the RAFT agent, keeps the overall radical concentration constant.

To investigate the capability of the immobilized CTA on reactive polymer coatings in mediating SI-RAFT polymerization, MMA was first polymerized from the S-CTA surface as a model monomer (Table 1, entry 1 and 2). Two different RAFT-agent-to-initiator ratios were used to better understand its influence on the growth of the polymer brushes. Ellipsometric measurements of the resulting PMMA film showed increasing thickness with reaction time (Fig. 3a). In general, an increase in the ratio of free RAFT agent to initiator is inversely proportional to the thickness of the polymer brush.

On increasing this ratio from 1 to 2.5, the thickness of the polymer brushes decreased showing that the thickness of the polymer brush layers was governed by the concentration of the free RAFT agent in solution. To understand the influence of the concentration of the free RAFT agent in solution on the controlled growth of the polymer brushes, the kinetics of the polymerization of MMA in solution were studied in detail. Samples were collected from the solution at intervals of 1 h. The polymers had relatively low dispersity ($Đ$) around 1.1–1.3 (Fig. 4a and b, triangles). The evolution of molecular weight with monomer conversion (Fig. 4a and b, squares) was linear, indicating a well-controlled polymerization. It is already well known that the solution polymerization kinetics and the surface polymerization kinetics can, and often are, quite different [57–59]. Thus, the solution polymerization and the molecular weights of the free polymers are used only as a guide.

XPS analysis of the PMMA film (Fig. 5) showed three signal components in the C 1s spectrum with binding energies at 285.0 eV for the C–C, C–H species, 286.7 eV for the C–O species and 289.1 eV for the O=C–O species [60]. O=C–O and C–O components showed a considerable increase in the intensity with increasing reaction time, as compared to the S-CTA surface. The observed increase in the O=C–O/(C–C, C–H) ratio as a function of reaction time correlated well with PMMA growth (Fig. 5b). After 1 h, the PMMA layer had a thickness of about 6 nm, whereas after 2 h, a thickness of more than 10 nm was measured, which explains the plateau observed for the O=C–O contribution after a reaction time of 2 h. For the control experiment, a PPX-alkyne surface without any immobilized RAFT agent was studied using similar reaction conditions (Fig. 5a, top). In this case, the intensity of the signals of the carbon components at 286.7 eV and 289.1 eV (Fig. 5b) were comparable to the data obtained from PPX-alkyne surface (Fig. S6, ESI†). They were also weaker than the intensity of the same signals of PMMA surface measured at 5 h. This result proves a negligible adsorption of PMMA solution polymers on the PPX-alkyne surface.

Fig. 1b shows the IRRAS spectra of PMMA. The bands from 1153 cm^{-1} to 1250 cm^{-1} are characteristic of C–O–C stretching. The band at 1381 cm^{-1} is characteristic of the α-methyl group vibrations. A sharp band at 1737 cm^{-1} is associated with the C=O stretch of the acrylate group. The band at 1445 cm^{-1} is due to the bending vibrations of the C–H bond of the $-CH_3$ group. The strong absorption bands at 2950 cm^{-1} and 2997 cm^{-1} are due to the C–H stretching vibrations of the $-CH_2$ groups and the $-CH_3$ groups,

Table 1
Summary of reaction conditions of SI-RAFT of MMA and MEDSAH.

Entry	Polymer	[M]:[CTA]:[I] (molar ratio)	Temperature (°C)	Solvent (v/v))	Time (h)	Thickness (nm)
1	PMMA	1150:1:1	70	DMF	6	45 ± 2.89
2	PMMA	1150:2.5:1	70	DMF	6	19 ± 1.39
3	PMEDSAH	7500:10:1	80	TFE:water (1:1)	8	20 ± 1.65

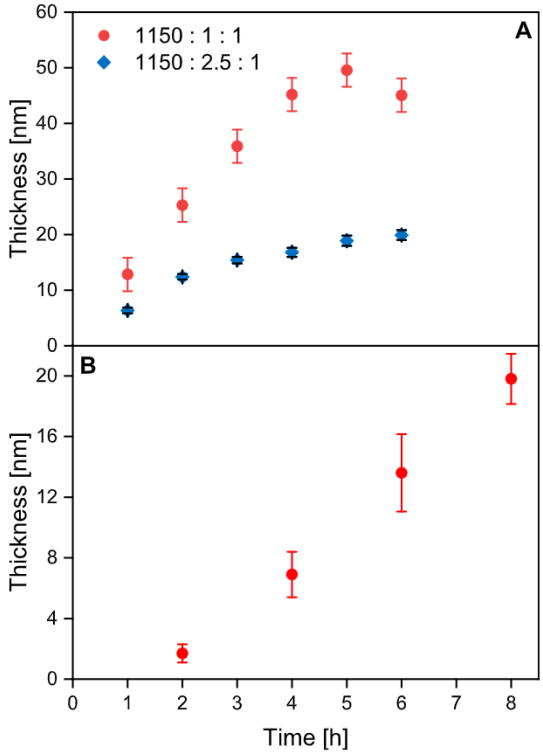

Fig. 3. Change in ellipsometric brush thicknesses with time for the (A) polymerization of MMA from silicon and gold surfaces at 70 °C. Reaction conditions = MMA/CTA/AIBN = 1150/1.0/1.0 (circle), MMA/CTA/AIBN = 1150/2.5/1.0 (diamond); (B) polymerization of MEDSAH from silicon and gold surfaces at 80 °C. Reaction conditions = MEDSAH/CTA/V501 = 7500/10/1.0.

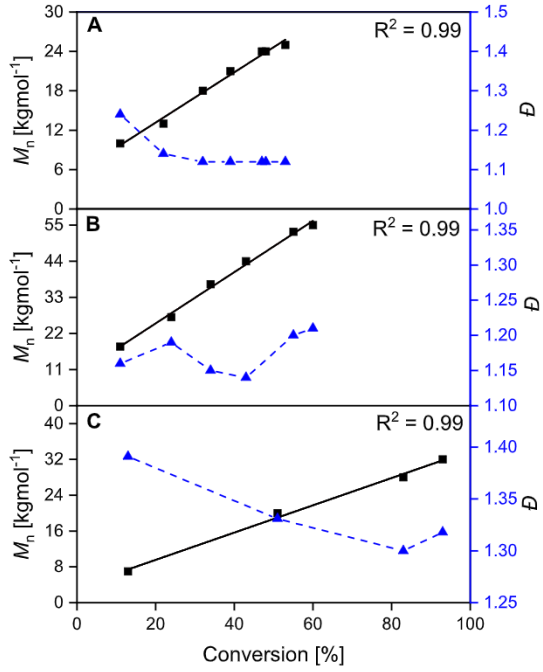

Fig. 4. Dependence of M_n (circles) and Đ (triangles) on the monomer conversion in the polymerization of MMA in DMF at 70 °C: (A) CTA/AIBN = 1/1, (B) CTA/AIBN = 2.5/1. (C) Dependence of M_n (circles) and Đ (triangles) on the monomer conversion in the polymerization of MEDSAH in TFE/water (1/1 v/v) at 80 °C.

respectively. The result of IRRAS confirms the successful grafting of PMMA polymer chains onto the PPX-alkyne surface [61].

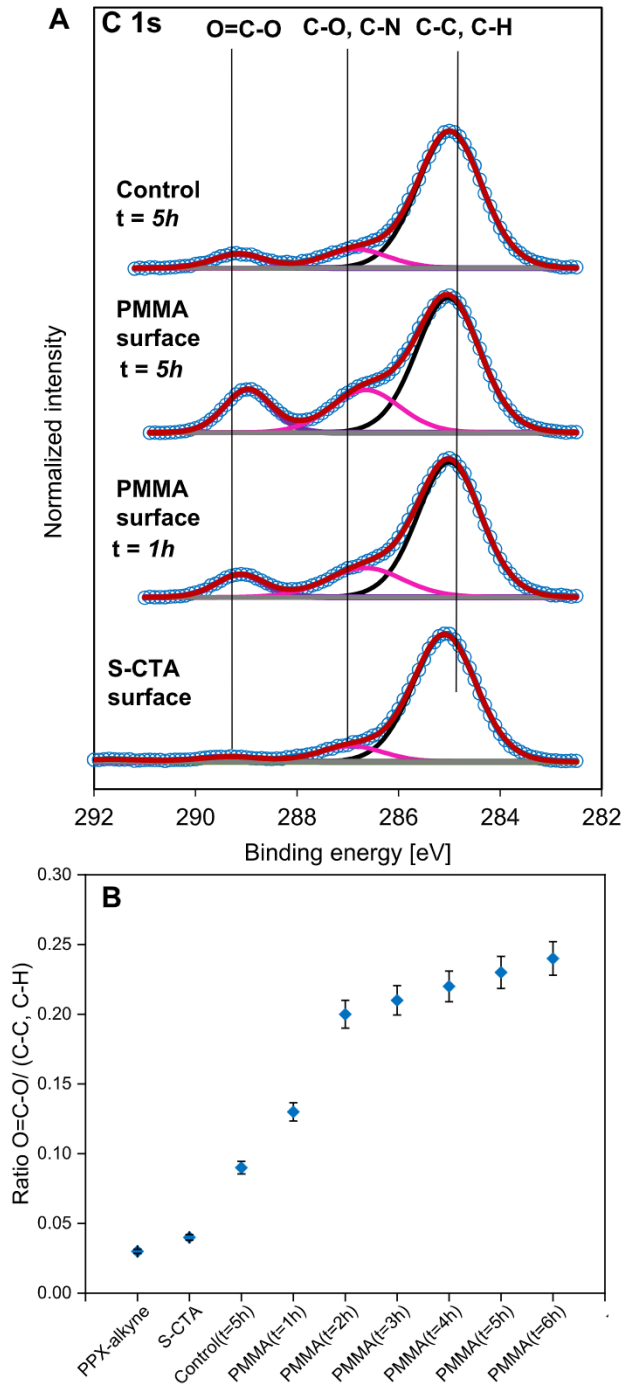

Fig. 5. (A) XPS high-resolution C 1s spectra of RAFT agent-decorated surface, PMMA surface (polymerization time = 1 h), PMMA surface (polymerization time = 5 h) and control sample. (B) XPS O–C=O/(C–C, C–H) ratio analysis before and after polymerization as a function of the reaction time.

We then modified the S-CTA surface by SI-RAFT polymerization of MEDSAH using the condition in Table 1, entry 3. V501 was used as a water-soluble initiator. Importantly, the molecular weight increased with conversion (Fig. 4c, squares) and Đ remained below 1.4 throughout the polymerization. The thickness increased with reaction time (Fig. 3b), demonstrating the grafting of PMEDSAH polymer on the surface. The XPS high-resolution C 1s scan (Fig. 6a) showed an increase in the signal intensity at 289.2 eV corresponding to the O–C=O group of PMEDSAH. In

addition, the signal at 286.7 eV is indicative of the C–O signal of the carboxyl group of PMEDSAH. From the N 1s spectrum in Fig. 6b, it is apparent that there is a quaternary ammonium $-N(CH_3)_2^+$ signal (402.8 eV) on the S-CTA surface after grafting of the PMEDSAH [62]. Further, doublets are discernible in the spectrum of the PMEDSAH surface (Fig. 6c). The most intensive S 2p doublet with S $2p_{3/2}$ at 168.0 eV corresponds to sulfonate $C-SO_3^-$ group in the side chains of PMEDSAH. The other two weaker S 2p doublets with S $2p_{3/2}$ at 164.2 eV and 163.0 eV are associated with the C–S and the C=S bonds of the dithioester end-group [54]. The N^+/SO_3^-/O–C=O ratio was ~1:1:1.

The growth of PMEDSAH brushes was also confirmed by IRRAS. As shown in Fig. 1c, characteristic vibrational bands at 1719 cm^{-1}, which are indicative of the C=O stretch were observed. The band at 1216 cm^{-1} can be assigned to the S=O stretching band. The band at 1450 cm^{-1} indicates the presence of methylene groups ($-CH_2-$). In addition, the band at 2928 cm^{-1} is indicative of C–H stretching vibrations [63]. Evidently, the sulfonate band is not present in PPX-alkyne surface. A larger contribution of the broad hydroxyl band between 3600 and 3200 cm^{-1} provides an indication that PMEDSAH absorbs moisture from the atmosphere.

The surface roughness of the different substrates was assessed (Fig. S7, ESI†). The root-mean-square (RMS) roughness (R_q) values were 1.1 nm, 2.3 nm and 3.6 nm for PPX-alkyne reactive polymer coating, PMMA and PMEDSAH films, respectively. All surfaces were homogenous and smooth and did not vary significantly ($t = 0.06$, $p > 0.05$). On the basis of the AFM study, we concluded that the surface morphologies show the clean and homogenous growth of the brushes from the reactive coatings.

Furthermore, the wettability of the PMEDSAH polymer was reduced, when compared to the PPX-alkyne reactive polymer coating (Fig. 7). In particular, the static water contact angle for PPX-alkyne was 103° ± 13°, the S-CTA surface was 82° and the PMEDSAH was 21 ± 5°. The difference in contact angles between S-CTA and PMEDSAH surfaces was statistically significant (*t*-test $p = 0.008$). This transition from hydrophobic to more hydrophilic surface properties occurred because of the grafted PMEDSAH chains on the surface. There was no change in wettability upon increasing the brush thickness. The statistical analysis showed no statistically significant difference between the varying thicknesses of PMEDSAH surfaces (*t*-test: $p > 0.05$).

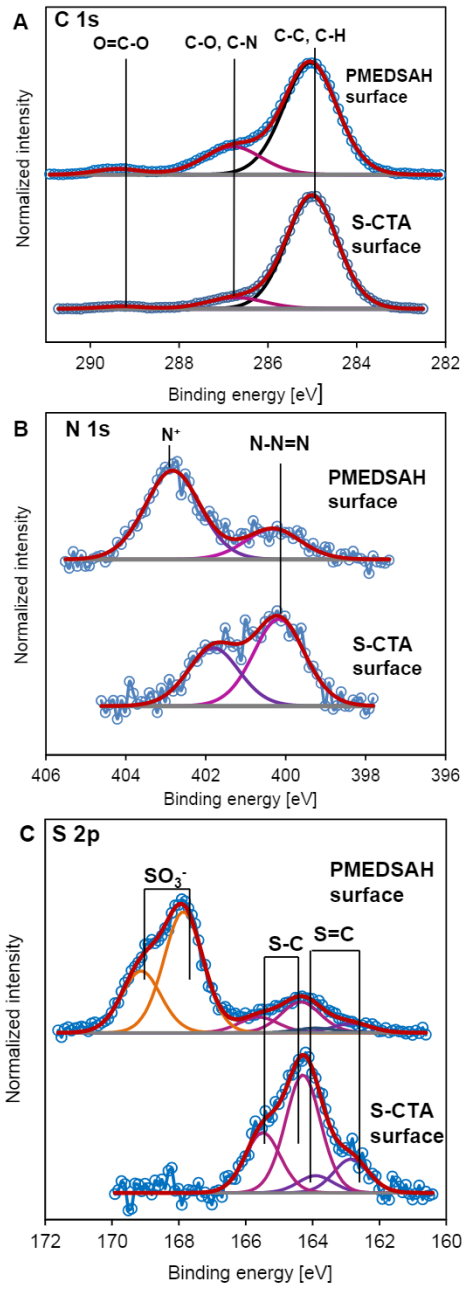

Fig. 6. High-resolution XPS spectra of C 1s (A) N 1s (B) and S 2p (C) for PMEDSAH film with a thickness of 20 nm grafted onto the RAFT agent-decorated surface via SI-RAFT polymerization.

4. Conclusions

In the current study, we reported the preparation of well-controlled PMMA (PDI < 1.3) as well as zwitterionic PMEDSAH polymers (PDI < 1.4) via RAFT polymerization from CVD-based surfaces. This system is advantageous in that the surface modification platform provides a potential to use versatile substrates, is stable and has a long shelf-life. This approach offers an effective way of preparing polymers without the use of copper and extends surface-RAFT polymerization to unconventional substrates that were not amenable to standard methods in this field. This facile surface modification strategy for the preparation of polymer surfaces enhances the materials toolbox for scientists and engineers engaged in biomaterials design.

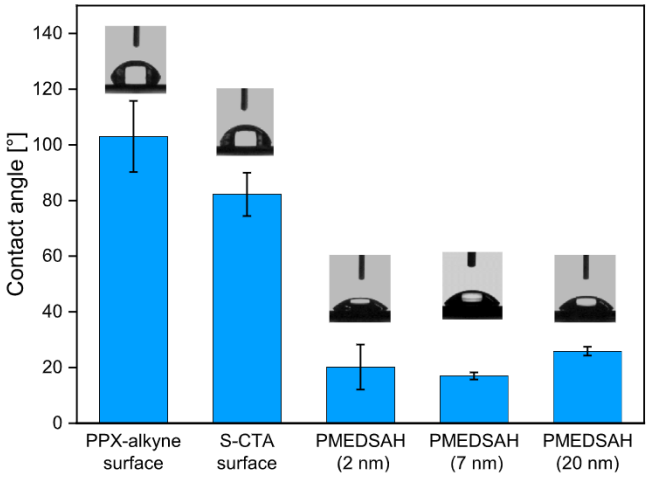

Fig. 7. Water contact angles on PPX-alkyne reactive polymer coating, RAFT agent-decorated surface and the PMEDSAH surfaces with different thicknesses of grafted PMEDSAH brushes.

Conflicts of interest

The authors declare no competing financial interest.

Acknowledgements

We like to thank Birgit Huber for her help with the SEC measurements, and Xiaopei Deng and Fan Xie for preparing PPX-alkyne surfaces. G.V. would like to thank Dr. Meike Koenig for AFM training. The authors acknowledge funding from the Helmholtz Association within the Biointerfaces Program of the KIT. L.B. and J.L. thank the German Science Foundation (DFG) for financial support within the frame of the collaborative research center SFB 1176 (Project B3). J.L. is grateful for support from the Defense Threat Reduction Agency (DTRA) through Grant HDTRA1-12-1-0039 and from the Army Research Office (ARO) under Grant W911NF-11-1-0251. This work was further supported by the Engineering Research Centers Program of the National Science Foundation under NSF Cooperative Agreement No. EEC-1647837.

Appendix A. Supplementary data

Supplementary data related to this article can be found at https://doi.org/10.1016/j.polymer.2018.06.073.

References

[1] A.J. Hackett, J. Malmström, J. Travas-Sejdic, Functionalization of conducting polymers for biointerface applications, Prog. Polym. Sci. 70 (2017) 18–33, https://doi.org/10.1016/j.progpolymsci.2017.03.004.
[2] A.E. Rodda, L. Meagher, D.R. Nisbet, J.S. Forsythe, Specific control of cell-material interactions: targeting cell receptors using ligand-functionalized polymer substrates, Prog. Polym. Sci. 39 (2014) 1312–1347, https://doi.org/10.1016/j.progpolymsci.2013.11.006.
[3] G.B. Jacobson, R. Shinde, C.H. Contag, R.N. Zare, Sustained release of drugs dispersed in polymer nanoparticles, Angew. Chem. 47 (2008) 7880–7882, https://doi.org/10.1002/anie.200802260.Sustained.
[4] R.H.G. Brinkhuis, A.J. Schouten, Thin-film behavior of poly(methyl methacrylates). 2. An FT-IR study of Langmuir-Blodgett films of isotactic PMMA, Macromolecules 24 (1991) 1496–1504, https://doi.org/10.1021/ma00007a010.
[5] J.O. Zoppe, N.C. Ataman, P. Mocny, J. Wang, J. Moraes, H.A. Klok, Surface-initiated controlled radical polymerization: state-of-the-art, opportunities, and challenges in surface and interface engineering with polymer brushes, Chem. Rev. 117 (2017) 1105–1318, https://doi.org/10.1021/acs.chemrev.6b00314.
[6] I. Choi, R. Suntivich, F.A. Plamper, C.V. Synatschke, A.H.E. Müller, V.V. Tsukruk, PH-controlled exponential and linear growing modes of layer-by-layer assemblies of star polyelectrolytes, J. Am. Chem. Soc. 133 (2011) 9592–9606, https://doi.org/10.1021/ja203106c.
[7] S. Edmondson, V.L. Osborne, W.T.S. Huck, Polymer brushes via surface-initiated polymerizations, Chem. Soc. Rev. 33 (2004) 14–22, https://doi.org/10.1039/b210143m.
[8] S.G. Boyes, A.M. Granville, M. Baum, B. Akgun, B.K. Mirous, W.J. Brittain, Polymer brushes - surface immobilized polymers, Surf. Sci. 570 (2004) 1–12, https://doi.org/10.1016/j.susc.2004.06.193.
[9] R. Barbey, L. Lavanant, D. Paripovic, N. Schuwer, C. Sugnaux, S. Tugulu, H.A. Klok, Polymer brushes via surface-initiated controlled radical polymerization: synthesis, characterization, properties, and applications, Chem. Rev. 109 (2009) 5437–5527, https://doi.org/10.1021/cr900045a.
[10] O. Azzaroni, I. Szleifer, Polymer and Biopolymer Brushes: for Materials Science and Biotechnology, vol. 1, John Wiley and Sons, NJ, USA, 2018.
[11] X. Fan, L. Lin, P.B. Messersmith, Cell fouling resistance of polymer brushes grafted from Ti substrates by surface-initiated polymerization: effect of ethylene glycol side chain length, Biomacromolecules 7 (2006) 2443–2448, https://doi.org/10.1021/bm060276k.
[12] B. Zhu, S. Edmondson, Polydopamine-melanin initiators for surface-initiated ATRP, Polymer 52 (2011) 2141–2149, https://doi.org/10.1016/j.polymer.2011.03.027.
[13] S. Perrier, 50th anniversary perspective: RAFT polymerization - a user guide, Macromolecules 50 (2017) 7433–7447, https://doi.org/10.1021/acs.macromol.7b00767.
[14] T. Bilgic, H.A. Klok, Surface-initiated controlled radical polymerization enhanced DNA biosensing, Eur. Polym. J. 62 (2015) 281–293, https://doi.org/10.1016/j.eurpolymj.2014.07.037.
[15] S. Beyazit, B. Tse Sum Bui, K. Haupt, C. Gonzato, Molecularly imprinted polymer nanomaterials and nanocomposites by controlled/living radical polymerization, Prog. Polym. Sci. 62 (2016) 1–21, https://doi.org/10.1016/j.progpolymsci.2016.04.001.
[16] B. Liu, D. Yang, H. Man, Y. Liu, H. Chen, H. Xu, W. Wang, L. Bai, A green Pickering emulsion stabilized by cellulose nanocrystals via RAFT polymerization, Cellulose 25 (2018) 77–85, https://doi.org/10.1007/s10570-017-1559-4.
[17] F. Ishizuka, R. Chapman, R.P. Kuchel, M. Coureault, P.B. Zetterlund, M.H. Stenzel, Polymeric nanocapsules for enzyme stabilization in organic solvents, Macromolecules (2018), https://doi.org/10.1021/acs.macromol.7b02377 acs.macromol.7b02377.
[18] M.R. Hill, E. Guégain, J. Tran, C.A. Figg, A.C. Turner, J. Nicolas, B.S. Sumerlin, Radical ring-opening copolymerization of cyclic ketene acetals and maleimides affords homogeneous incorporation of degradable units, ACS Macro Lett. 6 (2017) 1071–1077, https://doi.org/10.1021/acsmacrolett.7b00572.
[19] Z. Zheng, J. Ling, A.H.E. Müller, Revival of the R-group approach: a "CTA-shuttled" grafting from approach for Well-defined cylindrical polymer brushes via RAFT polymerization, Macromol. Rapid Commun. 35 (2014) 234–241, https://doi.org/10.1002/marc.201300578.
[20] K.A. Günay, N. Schüwer, H.A. Klok, Synthesis and post-polymerization modification of poly(pentafluorophenyl methacrylate) brushes, Polym. Chem. 3 (2012) 2186, https://doi.org/10.1039/c2py20162c.
[21] M. Zamfir, C. Rodriguez-Emmenegger, S. Bauer, L. Barner, A. Rosenhahn, C. Barner-Kowollik, Controlled growth of protein resistant PHEMA brushes via S-RAFT polymerization, J. Mater. Chem. B 1 (2013) 6027, https://doi.org/10.1039/c3tb20880j.
[22] M. Sakeye, J.H. Smatt, Comparison of different amino-functionalization procedures on a selection of metal oxide microparticles: degree of modification and hydrolytic stability, Langmuir 28 (2012) 16941–16950, https://doi.org/10.1021/la303925x.
[23] A. Zengin, T. Caykara, RAFT-mediated synthesis of poly[(oligoethylene glycol) methyl ether acrylate] brushes for biological functions, J. Polym. Sci. Part a Polym. Chem. 50 (2012) 4443–4450, https://doi.org/10.1002/pola.26250.
[24] M.D. Rowe, B.A.G. Hammer, S.G. Boyes, Synthesis of surface-initiated stimuli-responsive diblock copolymer brushes utilizing a combination of ATRP and RAFT polymerization techniques, Macromolecules 41 (2008) 4147–4157, https://doi.org/10.1021/ma800154c.
[25] M.R. Islam, L.G. Bach, T.S. Vo, T.N. Tran, K.T. Lim, Nondestructive chemical functionalization of MWNTs by poly(2- dimethylaminoethyl methacrylate) and their conjugation with CdSe quantum dots: synthesis, properties, and cytotoxicity studies, Appl. Surf. Sci. 286 (2013) 31–39, https://doi.org/10.1016/j.apsusc.2013.08.135.
[26] C.D. Grande, M.C. Tria, G. Jiang, R.R. Ponnapati, Y. Park, F. Zuluaga, R. Advincula, Grafting of polymers from electrodeposited macro-RAFT initiators on conducting surfaces, React. Funct. Polym. 71 (2011) 938–942, https://doi.org/10.1016/j.reactfunctpolym.2011.05.013.
[27] C.A. Kuliasha, R.L. Fedderwitz, P.R. Calvo, B.S. Sumerlin, A.B. Brennan, Engineering the surface properties of poly(dimethylsiloxane) utilizing aqueous RAFT photografting of acrylate/methacrylate monomers, Macromolecules 51 (2018) 306–317, https://doi.org/10.1021/acs.macromol.7b02575.
[28] X. Deng, J. Lahann, Orthogonal surface functionalization through bioactive vapor-based polymer coatings, J. Appl. Polym. Sci. 131 (2014) 40315–40324, https://doi.org/10.1002/app.40315.
[29] H.Y. Chen, J. Lahann, Designable biointerfaces using vapor-based reactive polymers, Langmuir 27 (2010) 34–48, https://doi.org/10.1021/la101623n.
[30] H.Y. Chen, Y. Elkasabi, J. Lahann, Surface modification of confined microgeometries via vapor-deposited polymer coatings, J. Am. Chem. Soc. 128 (2006) 374–380, https://doi.org/10.1021/ja057082h.
[31] J. Lahann, Vapor-based polymer coatings for potential biomedical applications, Polym. Int. 55 (2006) 1361–1370, https://doi.org/10.1002/pi.2098.
[32] J. Lahann, R. Langer, Novel poly(p-xylylenes): thin films with tailored chemical and optical properties, Macromolecules 35 (2002) 4380–4386, https://doi.org/10.1021/ma011769e.
[33] J. Lahann, Reactive polymer coatings for biomimetic surface engineering, Chem. Eng. Commun. 193 (2006) 1457–1468, https://doi.org/10.1080/00986440500511619.
[34] M. Gołda, M. Brzychczy-Włoch, M. Faryna, K. Engvall, A. Kotarba, Oxygen plasma functionalization of parylene C coating for implants surface: nanotopography and active sites for drug anchoring, Mater. Sci. Eng. C 33 (2013) 4221–4227, https://doi.org/10.1016/j.msec.2013.06.014.
[35] M. Cieślik, M. Kot, W. Reczyński, K. Engvall, W. Rakowski, A. Kotarba, Parylene coatings on stainless steel 316L surface for medical applications - mechanical and protective properties, Mater. Sci. Eng. C 32 (2012) 31–35, https://doi.org/10.1016/j.msec.2011.09.007.
[36] S.V. Dorozhkin, Calcium orthophosphate coatings on magnesium and its biodegradable alloys, Acta Biomater. 10 (2014) 2919–2934, https://doi.org/10.1016/j.actbio.2014.02.026.
[37] C.P. Tan, H.G. Craighead, Surface engineering and patterning using parylene for biological applications, Materials 3 (2010) 1803–1832, https://doi.org/10.3390/ma3031803.
[38] J. Lahann, D. Klee, H. Hocker, Chemical vapour deposition polymerization of substituted [2.2]paracyclophanes, Macromol. Rapid Commun. 19 (1998) 441–444, https://doi.org/10.1002/marc.1998.030190901.
[39] H. Nandivada, H.Y. Chen, L. Bondarenko, J. Lahann, Reactive polymer coatings that "click,", Angew. Chem. Int. Ed. 45 (2006) 3360–3363, https://doi.org/10.1002/anie.200600357.

[40] X. Deng, T.W. Eyster, Y. Elkasabi, J. Lahann, Bio-orthogonal polymer coatings for co-presentation of biomolecules, Macromol. Rapid Commun. 33 (2012) 640–645, https://doi.org/10.1002/marc.201100819.
[41] A. Ross, H. Durmaz, K. Cheng, X. Deng, Y. Liu, J. Oh, Z. Chen, J. Lahann, Selective and reversible binding of thiol-functionalized biomolecules on polymers prepared via chemical vapor deposition polymerization, Langmuir 31 (2015) 5123–5129, https://doi.org/10.1021/acs.langmuir.5b00654.
[42] H. Nandivada, H.Y. Chen, J. Lahann, Vapor-based synthesis of poly[(4-formyl-p-xylylene)-co-(p-xylylene)] and its use for biomimetic surface modifications, Macromol. Rapid Commun. 26 (2005) 1794–1799, https://doi.org/10.1002/marc.200500449.
[43] J. Lahann, I.S. Choi, J. Lee, K.F. Jensen, R. Langer, A new method toward microengineered surfaces based on reactive coating, Angew. Chem. Int. Ed. 40 (2001) 3166–3169, https://doi.org/10.1002/1521-3773(20010903)40:17<3166::AID-ANIE3166>3.0.CO;2-#.
[44] H.Y. Chen, M. Hirtz, X. Deng, T. Laue, H. Fuchs, J. Lahann, Substrate-independent dip-pen nanolithography based on reactive coatings, J. Am. Chem. Soc. 132 (2010) 18023–18025, https://doi.org/10.1021/ja108679m.
[45] Z. Li, T.S. Seo, J. Ju, 1,3-Dipolar cycloaddition of azides with electron-deficient alkynes under mild condition in water, Tetrahedron Lett. 45 (2004) 3143–3146, https://doi.org/10.1016/j.tetlet.2004.02.089.
[46] S. Jiang, Z. Cao, Ultralow-fouling, functionalizable, and hydrolyzable zwitterionic materials and their derivatives for biological applications, Adv. Mater. 22 (2010) 920–932, https://doi.org/10.1002/adma.200901407.
[47] L.G. Villa-Diaz, H. Nandivada, J. Ding, N.C. Nogueira-de-Souza, P.H. Krebsbach, K.S. O'Shea, J. Lahann, G.D. Smith, Synthetic polymer coatings for long-term growth of human embryonic stem cells, Nat. Biotechnol. 28 (2010) 581–583, https://doi.org/10.1038/nbt.1631.
[48] K.L. Parry, A.G. Shard, R.D. Short, R.G. White, J.D. Whittle, A. Wright, ARXPS characterisation of plasma polymerised surface chemical gradients, Surf. Interface Anal. 38 (2006) 1497–1504, https://doi.org/10.1002/sia.2400.
[49] J.H. Scofield, Hartree-Slater subshell photoionization cross-sections at 1254 and 1487 eV, J. Electron. Spectrosc. Relat. Phenom. 8 (1976) 129–132, https://doi.org/10.1016/0368-2048(76)80015-1.
[50] X. Deng, C. Friedmann, J. Lahann, Bio-orthogonal "double-click" chemistry based on multifunctional coatings, Angew. Chem. Int. Ed. 50 (2011) 6522–6526, https://doi.org/10.1002/anie.201101581.
[51] B.D. Ratner, A.S. Hoffman, F.J. Schoen, J.E. Lemons, Biomaterials Science, Academic Press, 1996, https://doi.org/10.1016/B978-0-08-087780-8.00148-0.
[52] M.D. De Tercero, M. Bruns, I.G. Martínez, M. Türk, U. Fehrenbacher, S. Jennewein, L. Barner, Continuous hydrothermal synthesis of in situ functionalized iron oxide nanoparticles: a general strategy to produce metal oxide nanoparticles with clickable anchors, Part. Part. Syst. Char. 30 (2013) 229–234, https://doi.org/10.1002/ppsc.201200109.
[53] J. Eisenblaetter, M. Bruns, U. Fehrenbacher, L. Barner, C. Barner-Kowollik, Synthesis of polymers with phosphorus containing side chains via modular conjugation, Polym. Chem. 4 (2013) 2406, https://doi.org/10.1039/c3py00103b.
[54] J.F. Moulder, W.F. Stickle, P.E. Sobol, K.D. Bomben, Handbook of X-ray Photoelectron Spectroscopy, Eden Prarie (MN), 1992, https://doi.org/10.1002/sia.740030412.
[55] Y. Tsujii, M. Ejaz, K. Sato, A. Goto, T. Fukuda, Mechanism and kinetics of RAFT-mediated graft polymerization of styrene on a solid surface. 1. Experimental evidence of surface radical migration, Macromolecules 34 (2001) 8872–8878, https://doi.org/10.1021/ma010733j.
[56] S. Perrier, P. Takolpuckdee, C.A. Mars, Reversible addition-fragmentation chain transfer polymerization mediated by a solid supported chain transfer agent, Macromolecules 38 (2005) 6770–6774, https://doi.org/10.1021/ma0506886.
[57] E. Marutani, S. Yamamoto, T. Ninjbadgar, Y. Tsujii, T. Fukuda, M. Takano, Surface-initiated atom transfer radical polymerization of methyl methacrylate on magnetite nanoparticles, Polymer 45 (2004) 2231–2235, https://doi.org/10.1016/j.polymer.2004.02.005.
[58] M. Barsbay, O. Güven, T.P. Davis, C. Barner-Kowollik, L. Barner, RAFT-mediated polymerization and grafting of sodium 4-styrenesulfonate from cellulose initiated via γ-radiation, Polymer 50 (2009) 973–982, https://doi.org/10.1016/j.polymer.2008.12.027.
[59] B. Deng, E.F. Palermo, Y. Shi, Comparison of chain-growth polymerization in solution versus on surface using reactive coarse-grained simulations, Polymer 129 (2017) 105–116, https://doi.org/10.1016/j.polymer.2017.09.048.
[60] G. Beamson, D. Briggs, High Resolution XPS of Organic Polymers: the Scienta ESCA300 Database, Wiley, Chichester [England]; New York, 1992.
[61] S. Dirlikov, J. Koenig, Infrared spectra of poly (methyl methacrylate) labeled with oxygen-18, Appl. Spectrosc. 33 (1979) 551–555.
[62] C. Gabler, C. Tomastik, J. Brenner, L. Pisarova, N. Doerr, G. Allmaier, Corrosion properties of ammonium based ionic liquids evaluated by SEM-EDX, XPS and ICP-OES, Green Chem. 13 (2011) 2869, https://doi.org/10.1039/c1gc15148g.
[63] P.J. Linstrom, W.G. Mallard, NIST Chemistry WebBook, NIST Standard Reference Database Number 69, 2014 doi:citeulike-article-id:3211271.